



Multiphase computed tomography angiography derived from computed tomography perfusion data for the differential diagnosis of intracranial aneurysm and infundibular dilation

Huaiyu Zhang^{1,2,3^}, Wenhao Liu³, Zhuang Zhang^{3,4}, Zhiqiang Yan³, Xiaoyong Tao⁵, Feng Qiu⁵, Yuangang Qiao³, Lirong Zhang¹

¹Department of Radiology, Aerospace Center Hospital, Beijing, China; ²Department of Radiology, PLA Rocket Force Characteristic Medical Center, Beijing, China; ³Department of Radiology, The 8th Medical Center of Chinese PLA General Hospital, Beijing, China; ⁴Department of Graduate, Hebei North University, Zhangjiakou, China; ⁵Department of Neurology, The 8th Medical Center of Chinese PLA General Hospital, Beijing, China

Contributions: (I) Conception and design: Y Qiao, H Zhang; (II) Administrative support: X Tao, F Qiu; (III) Provision of study materials or patients: Z Zhang, W Liu, Y Qiao, Z Yan, X Tao, F Qiu; (IV) Collection and assembly of data: Z Zhang, W Liu, Y Qiao; (V) Data analysis and interpretation: H Zhang, L Zhang; (VI) Manuscript writing: All authors; (VII) Final approval of manuscript: All authors.

Correspondence to: Lirong Zhang, MM. Department of Radiology, Aerospace Center Hospital, Beijing 100049, China. Email: LirongZhang01@163.com; Yuangang Qiao, MM. Department of Radiology, The 8th Medical Center of Chinese PLA General Hospital, Beijing 100091, China. Email: qiaoyg1@163.com.

Background: As infundibular dilation (ID) is less likely to cause hemorrhage or other clinical sequelae than an intracranial aneurysm (IA) and treating infundibulum itself may put the patient at unnecessary risk for stroke, it is important to distinguish between the ID and IA. Given the limitations of conventional single-phase computed tomography angiography (sCTA) to show small branches of intracranial arteries, the application of multiphase computed tomography angiography (mCTA) for identification seems promising. Our main objective was to evaluate whether using mCTA derived from computed tomography perfusion (CTP) data can improve distinction between IA and ID.

Methods: A total of 35 patients diagnosed with IA or ID of the posterior communicating artery at its junction with the internal carotid artery junction (ICA–PComA) by sCTA at the 8th Medical Center of Chinese PLA General Hospital between January 2019 and May 2022 were retrospectively selected. All patients underwent CTP. The simulated mCTA was reconstructed from 0.75 mm CTP data for assessment of vascular branches. All data were processed separately by 2 CTA post-processors; 2 observers diagnosed IA and ID by source and volume rendering (VR) images of sCTA and VR images of mCTA, and compared the diagnostic efficacy of source and VR images of sCTA with VR images of mCTA.

Results: The quality of the reconstructed images was more consistent between the 2 post-processors mCTA (K=0.856) than sCTA (K=0.648). The sensitivity, specificity, positive predictive value (PPV), negative predictive value (NPV), and accuracy of the source image for ID identification were 78.9%, 86.7%, 84.2%, 81.3%, and 80.0% for sCTA, 73.7%, 81.2%, 82.3%, 72.2%, and 77.2% for the VR image of sCTA, and 94.7%, 87.5%, 90.0%, 93.3%, and 91.4% for the VR image based on mCTA, respectively. The net reclassification index (NRI) of mCTA for VR and the source image of sCTA was 0.273 and 0.220, respectively. VR base on mCTA was on average better than VR and the source image of sCTA at differentiating ID from IA (P=0.005 and P=0.001, respectively).

Conclusions: Compared to sCTA, mCTA is more helpful in improving the distinction of ID and IA.

[^] ORCID: 0000-0002-5561-2210.

Keywords: Infundibular dilation (ID); intracranial aneurysm (IA); multiphase computed tomography angiography (mCTA); computed tomography perfusion (CTP); single-phase computed tomography angiography (sCTA)

Submitted Feb 20, 2023. Accepted for publication Jul 19, 2023. Published online Aug 15, 2023.

doi: 10.21037/qims-23-211

View this article at: <https://dx.doi.org/10.21037/qims-23-211>

Introduction

In the general population, the prevalence of unruptured intracranial aneurysms (IA) is approximately 2–3% (1). Aneurysmal subarachnoid hemorrhage (SAH) caused by IA is a devastating subset of strokes and results in serious disability (2). Infundibular dilation (ID) is a funnel-shaped widening of the origin of the cerebral arteries, usually at origin of the posterior communicating artery at its junction with the internal carotid artery (ICA–PComA) (3). The prevalence of IDs is 7–25% as detected by angiography or autopsy, and they are usually considered normal anatomical variants (4). As ID is less likely to cause hemorrhage or other clinical sequelae than an aneurysm and treating infundibulum itself may put the patient at unnecessary risk for stroke (5), it is important to distinguish between the 2 entities.

The gold standard for distinguishing ID from IA is digital subtraction angiography (DSA), but non-invasive imaging modalities such as magnetic resonance angiography (MRA), computed tomography angiography (CTA), and 3-dimensional (3D) rotational angiogram (3DRA) have been used in the differential diagnosis (6). The ability to demonstrate the branch arising out of infundibulum apex is helpful in diagnosis (7). CTA is less time consuming and information on the status of collaterals can be obtained by appropriate acquisition and reconstruction methods. However, conventional single-phase CTA (sCTA) depicts the cerebral circulation at a single snapshot which depends on the timing of CTA acquisition after contrast material injection, which may lead to inaccurate estimation of the circulation (8). Computed tomography perfusion (CTP) is increasingly being used in clinical practice for the assessment of different neurovascular disorders as a noninvasive method and provides an option to derive 4-dimensional (4D) CTA (9). CTA images of specific periods can also be generated by extracting and summing information, producing simulated multiphase CTA (mCTA) to assess collaterals in addition to CTP data (10).

In this study, we aimed to evaluate whether the

application of mCTA could help in the differential diagnosis of IDs from IA. We present this article in accordance with the STARD reporting checklist (available at <https://qims.amegroups.com/article/view/10.21037/qims-23-211/rc>).

Methods

Patients

This retrospective study enrolled 39 patients diagnosed with IA or IDs at the ICA–PComA junction by sCTA from the 8th Medical Center of Chinese PLA General Hospital between January 2019 to May 2022. Individuals were excluded if CTA data was missing, or only follow-up data was available without DSA confirmation. The baseline patient characteristics variables collected included age, gender, systolic blood pressure (SBP), diastolic blood pressure (DBP), hyperlipidemia, smoking, and history of drinking. The study was conducted in accordance with the Declaration of Helsinki (as revised in 2013). The study was approved by the Institutional Review Board of Chinese PLA General Hospital (No. HZKY-PJ-2020-38) and the requirement for individual consent for this retrospective analysis was waived. The participants formed a convenience sample, with the sample size of this study being determined based on feasibility considerations.

Single-phase CTA

The CTA examinations were performed using 320 multi-slice computed tomography (CT) [Aquilion One; Toshiba Medical Systems Corp, Otawara, Japan; 0.5 mm thickness; 75 ms gantry rotation time, 120 kV, 510 mAs, CT dose index (CTDI_{vol}) of 231.9 mGy, and dose-length product (DLP) of 3,244.8 mGy·cm]. The scanning range was from foramen magnum to skull vertex. Scanning was performed using a bolus-tracking technique. In total, 60 mL of iopromide (Ultravist 370; Bayer Schering, Berlin, Germany) was administered at 6 mL/s through an 18-gauge needle positioned in a peripheral vein.

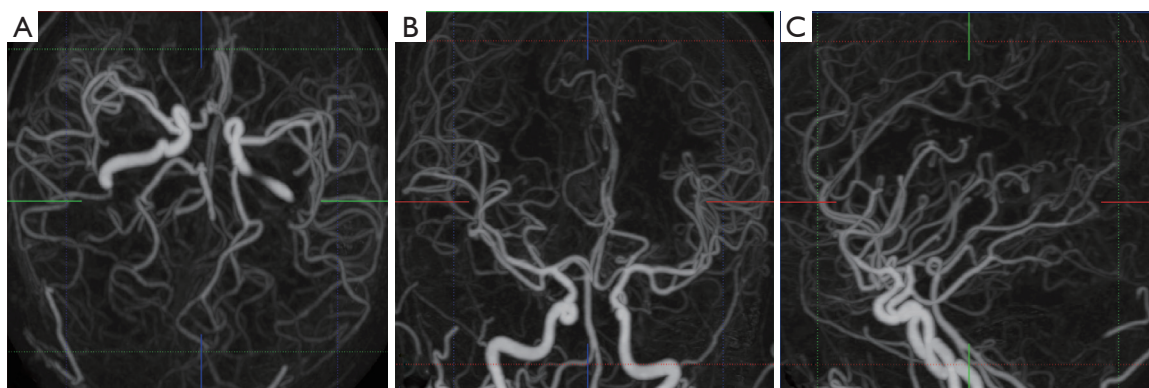


Figure 1 Diagram of the range of reconstruction. (A,B) Axial and coronal MIP images, with reconstructions including the distal branch margins of the middle cerebral artery on both sides. (C) A sagittal MIP image with a reconstruction that includes the distal branch margins of the anterior and posterior cerebral arteries. MIP, maximum intensity projection.

Multiphase CTA derived from CTP

The dynamic volume interval mode of 320 multi-slice CT was employed, comprising multiple volume acquisitions of the entire skull in an axial fashion. The 320-detector row CT enables 160 mm z-axis coverage with slice thickness of 0.75 mm, a field of view (FOV) of 220×220 mm and a 512×512 slice matrix. The scanning range was from foramen magnum to skull vertex. A total of 3 sequences were conducted and 19 time-phases were acquired. The first sequence was a mask sequence consisting of 1 time-phase (120 kV, 50 mA). The second sequence was dynamic angiography, which consists of 3 parts. For the first part, 3 time-phases are scanned and acquired at 2 seconds intervals. Acquisition of the second part was performed after an interval of 4.75 seconds, scanning 6 time-phases, each 2 seconds apart. The last part was acquired after an interval of 4.75 seconds, scanning 4 time-phases, each acquired every 2 seconds. A total of 13 time-phases (120 kV, 300 mA) were generated, the interval duration for the third sequence was longer in order to obtain perfusion data for the entire brain; 5 time-phases were generated at rate of 1 per 4.5 seconds (120 kV, 300 mA). The CTDIvol was 47.1 mGy per time-phase, and the DLP was 754.4 mGy-cm, for a total CTDIvol of 895.9 mGy, and a total DLP of 14,333.6 mGy-cm. Iopromide (60 mL of 370 mg/mL, Ultravist 370) was injected intravenously with an automatic injector at a rate of 6 mL/s. We selected only the second sequence (dynamic angiography) for 3D reconstruction. The scanning range was from foramen magnum to skull vertex. Scanning was conducted using a bolus-tracking technique.

Image post-processing

The post-processing of mCTA was all performed in Vitrea Workstation (version 6.5.1; Canon Medical, Otawara, Japan) independently by 2 post-processors; 3 time-phases were selected (peak arterial, peak venous, and late venous phases) for 3D reconstruction using 4D-vascular protocol, and after automatic bone removal, the entire intracranial artery was displayed using the 3D BOX tool, and selected axial, coronal, and sagittal maximum intensity projection (MIP) images of the peak arterial phase, including all distal branches of the anterior, middle, and posterior cerebral arteries (*Figure 1*). The Vitrea Workstation was also used for sCTA, selecting the same reconstruction range. The mCTA and sCTA reconstructed images are displayed in *Figure 2*.

Image quality and analysis

Volume rendering (VR) images of mCTA and sCTA image quality were scored independently by 2 observers (Dr. Y.Q. and Dr. X.T.) on a 5-point scale [0–4], used as a subjective assessment of image quality in the current scanning modality and to assess the consistency of image reconstruction between the 2 post-processors. The scoring criteria were as follows: score 4: clear display of the main trunk and branches of the intracranial arteries and clear display of the lesion, with no bony structures obscuring observation; score 3: intracranial artery trunk clearly displayed, branches poorly displayed, lesions clearly displayed, no bony structures obscuring observation; score 2: the main trunk of the intracranial artery is clear, branches and lesions are indistinct and not obscured by bony structures; score 1: the main trunk of the

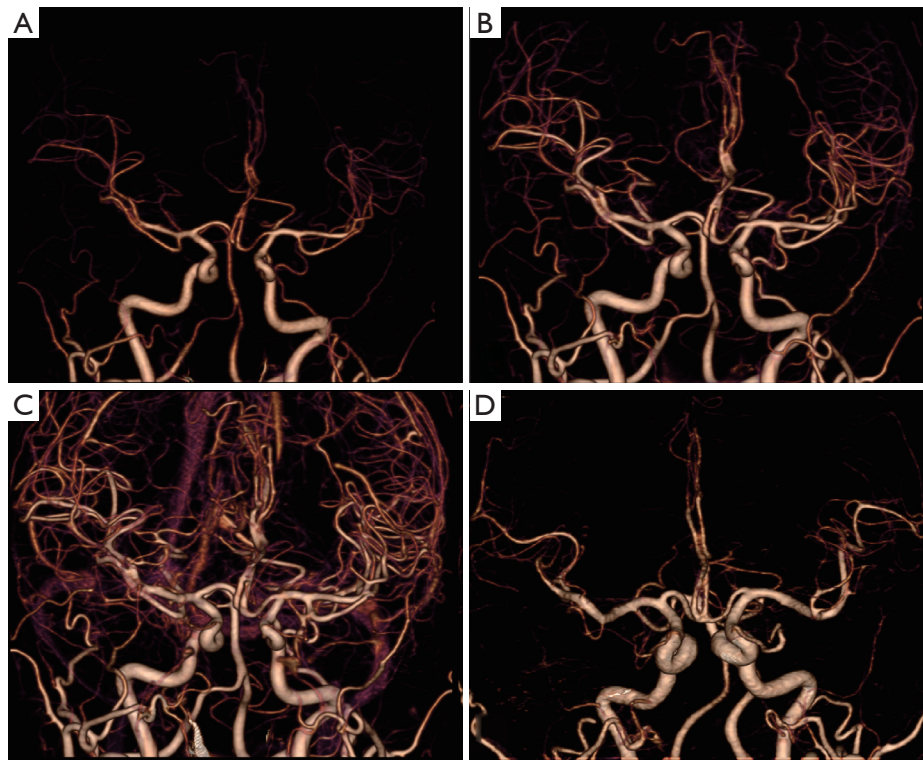


Figure 2 mCTA and sCTA reconstructed images. (A-C) Represent the peak arterial, peak venous, and late venous phases, respectively. (D) Displays an sCTA reconstruction. (A-C) Demonstrate the dynamic information of the blood flow, with the arterial branches progressing from few to many, to the cerebral venous system being visualized. MCTA, multiphase computed tomography angiography; sCTA, single-phase computed tomography angiography.

intracranial artery is clear, branches and lesions are poorly visualized, with bony structures obscuring them; score 0: the image cannot be used for observation at all. The 3-point method was used to evaluate the observer's confidence in distinguishing ID and IA: (I) easy to judge, (II) difficult to judge, and (III) unable to judge (6). IA or ID were diagnosed independently by 2 observers (Dr. YQ and Dr. WL). Any interobserver disagreement was resolved by consensus. A second observation was made after an interval of 3 months.

Statistical analysis

The agreement of the 2 post-processors image quality and interobserver were determined by calculation of kappa (K) values. The strength of agreement was rated as follows: 0= poor, 0–0.20= slight, 0.21–0.40= fair, 0.41–0.60= moderate, 0.61–0.80= substantial, and 0.81–1.00= almost perfect (11). Sensitivity, specificity, accuracy, and positive predictive value (PPV) and negative predictive value (NPV) of mCTA for differential diagnosis of ID were calculated using the

consensus DSA evaluation as the reference standard. The net reclassification index (NRI) (12) was used to evaluate the differential efficacy of mCTA and sCTA. Mean and standard deviation (SD) were used to describe quantitative variables, whereas in the case of qualitative variables, percentages were used. First, a bivariate analysis was carried out, using Student's *t*-test for independent samples or Mann-Whitney U-test for quantitative variables, whereas the chi-square test was used for qualitative variables. Wilcoxon matched-pairs signed-rank test and Fisher's exact probability test were used to examine the ability of different images to distinguish between ID and IA. A P value <0.05 was considered statistically significant. All statistical analyses were performed using the SPSS 26.0 statistical software package (IBM Corp, Armonk, NY, USA).

Results

The patient enrollment flow diagram is shown in *Figure 3*. Of the 39 healthy individuals enrolled in this study,

4 patients were excluded due to follow-up only without DSA confirmation (n=3) and CTA data loss (n=1). Therefore, 35 patients with 35 protrusions at the ICA-PCoM junction were included in this study. There were 16 patients with IA, 7 (43.8%) males and 9 (56.2%) females, aged 42–86 years, with a mean age of 59±14 years, SBP 110–133 mmHg, with a mean of 123.5±2.5 mmHg, DBP 76–101 mmHg, with a mean of 86.2±1.7, 9 (56.2%) patients with hyperlipidemia, 6 (37.5%) patients had a history of smoking, and 7 (43.8%) patients had a history of drinking. There were 19 patients with ID, 11 (57.9%) males and 8 (42.1%) females, aged 39–78 years, with a mean age of 57±12 years, SBP 112–142, with a mean of 127.2±2.2 mmHg, DBP 77–103, with a mean of 90.9±1.8, 12 (63.2%) patients

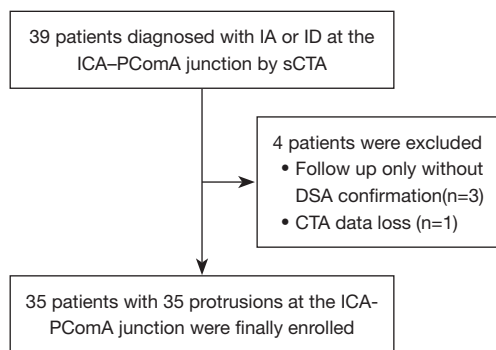


Figure 3 The patient selection flowchart. IA, intracranial aneurysm; ID, infundibular dilation; ICA-PCoM, posterior communicating artery at its junction with the internal carotid artery; sCTA, single-phase computed tomography angiography; DSA, digital subtraction angiography; CTA, computed tomography angiography.

with hyperlipidemia, 11 (57.9%) patients with a history of smoking, and 11 (57.9%) patients with a history of drinking (Table 1). All patients underwent sCTA and CTP scans and were successfully reconstructed in 3D using volumetric reproduction techniques. The Kappa value between the 2 CTA post-processors for the sCTA images was 0.648 and 0.856 for mCTA. The results of 2 retrospective observations of mCTA and sCTA by the 2 observers were identical.

The sensitivity, specificity, PPV, NPV, and accuracy of the source image for ID identification were 78.9%, 86.7%, 84.2%, 81.3%, and 80.0% for sCTA, 73.7%, 81.2%, 82.3%, 72.2%, and 77.2% for the VR image of sCTA, and 94.7%, 87.5%, 90.0%, 93.3%, and 91.4% for the VR image base on mCTA, respectively (Table 2). On VR image of sCTA, 5 ID were misdiagnosed as IA and 3 IA were misdiagnosed as ID; on the source image, 4 ID were misdiagnosed as IA and 3 IA were misdiagnosed as ID, whereas on mCTA 1 ID was misdiagnosed as an IA and 2 IA were misdiagnosed as ID, with an NRI of 0.273 [95% confidence interval (CI): -0.003 to 0.566] and 0.220 (95% CI: 0.048–0.442). The results of Fisher's exact test showed a higher proportion of applied VR of mCTA images identifying ID in easy to judge areas relative to the VR images of sCTA (P=0.004) and the original images (P=0.045). The Wilcoxon signed-rank test showed that VR images of mCTA was on average better than the VR images of sCTA (P=0.005) and the source images (P=0.001) at differentiating ID from IA (Table 3).

Discussion

Funnel-shaped symmetrical enlargements at the origin of the PcoM without an aneurysmal neck are also known as ID (13), and are generally considered a typically

Table 1 Characteristics of the patients

Variables	IA	ID	P value
Age (years)	59±14	57±12	0.54
Male/female	7/9	11/8	0.51
Systolic blood pressure (mmHg)	123.5 (±2.5)	127.2 (±2.2)	0.30
Diastolic blood pressure (mmHg)	86.2 (±1.7)	90.9 (±1.8)	0.07
Hyperlipidemia	9 (56.2)	12 (63.2)	0.73
Smoking	6 (37.5)	11 (57.9)	0.32
History of drinking	7 (43.8)	11 (57.9)	0.51

The table presents the baseline information for total patients, IA, and ID. P value present the difference between the IA and ID. Values are mean (SD), n (%). IA, intracranial aneurysm; ID, infundibular dilation.

Table 2 Diagnostic performance of VR images of mCTA with sCTA source images and VR images in distinguishing IA and ID at the ICA–PCoMA

Procedure	Sensitivity	Specificity	PPV	NPV	Accuracy
The source image of sCTA	78.9%	86.7%	84.2%	81.3%	80.0%
VR of sCTA	73.7%	81.2%	82.3%	72.2%	77.2%
VR of mCTA	94.7%	87.5%	90.0%	93.3%	91.4%

VR, volume rendering; mCTA, multiphase computed tomography angiography; sCTA, single-phase computed tomography angiography; IA, intracranial aneurysm; ID, infundibular dilation; ICA–PCoMA, posterior communicating artery at its junction with the internal carotid artery; PPV, positive predictive value; NPV, negative predictive value.

Table 3 Comparison of VR image and source image of sCTA and VR image of mCTA for differentiation between IA and ID

Procedure	Scale of difficulty for judgement			Total	χ^2	P value	95% CI	Z	P value	95% CI*
	1	2	3							
VR image of mCTA	29	5	1	35	Ref	Ref	Ref	Ref	Ref	Ref
VR image of sCTA	16	17	2	35	9.737	0.004**	1.661–12.361	2.837	0.005**	0.000–0.500
The source image of sCTA	20	13	2	35	5.543	0.045**	1.049–7.120	5.385	0.001**	0.000–0.500

χ^2 : statistics of Fisher's exact probability test; 95% CI: represents the 95% confidence interval of the χ^2 of Fisher's exact probability test; Z: statistics of Wilcoxon matched pairs signed-rank test; 95% CI*: represents the 95% confidence interval of the P value of Wilcoxon matched pairs signed-rank test; **, indicates a statistically significant result. VR, volume rendering; sCTA, single-phase computed tomography angiography; mCTA, multiphase computed tomography angiography.

benign anatomical variation (5). ID typically presents as an adult-type PCoMA and may represent the remnants of a previously dominant fetal vessel (14). Even so, some potential risks of arterial cones have been reported. Some studies have reported the progression of ID to a saccular aneurysm (15–17). In addition, some studies have reported SAH due to rupture of ID without progression to a saccular aneurysm (18–20). Since the risk of SAH from ID is low and the treatment of IDs themselves can easily lead to unnecessary strokes in patients, a follow-up strategy is often used in clinical practice. IA is a serious risk factor for SAH and some patients have a poor prognosis that requires an aggressive treatment strategy, therefore, the differentiation between ID and IA is a major clinical focus.

The gold standard for the identification of ID and IA is DSA. The invasive nature of DSA, as well as the possible side effects and complications caused by contrast medium and radiation, such as a sustained neurological dysfunction, make DSA unsuitable for screening and repeat follow-up (21–23). A non-invasive and accurate examination is a clinical necessity. A number of non-invasive examinations have served well in the identification of ID and IA. Min *et al.* performed CTA using a 4-detector CT scanner in

107 cases of ICA–PCoMA protrusions (37 aneurysms and 70 IDs) (7). Satoh *et al.* used imaging of 3D MRA for differential diagnosis of ID and IA of the internal carotid artery (ICA) (24). Jang *et al.* presented a preliminary discussion on the identification of ID and IA using 3DRA (6). CTA is routinely used clinically. Typical ID imaging features show a widened triangular or conical shape, with a basal maximum diameter generally less than 3 mm, lack of a neck, and a branching artery arising from its apex; in contrast, IA typically present as round or irregularly dilated, aneurysmal necks with a maximum diameter of more than 3 mm and branching arteries arising from the base (7). There is a significant overlap in lesion morphology and size between these 2 vascular lesions. ID may become rounded with increased size (25). Shi *et al.* reported that 7 of 48 IDs (14.6%) were larger than 3 mm (26). Accurate visualization of PCoMA is essential to differentiate ID from IA (7). However, sCTA relies on the timing of the acquisition of angiography and has disadvantages in demonstrating the small branches of the intracranial arteries (7,27). The potential for inadequate filling of the contrast medium on the sCTA is higher due to the bidirectional flow within the PCoMA from the distal ICA and proximal

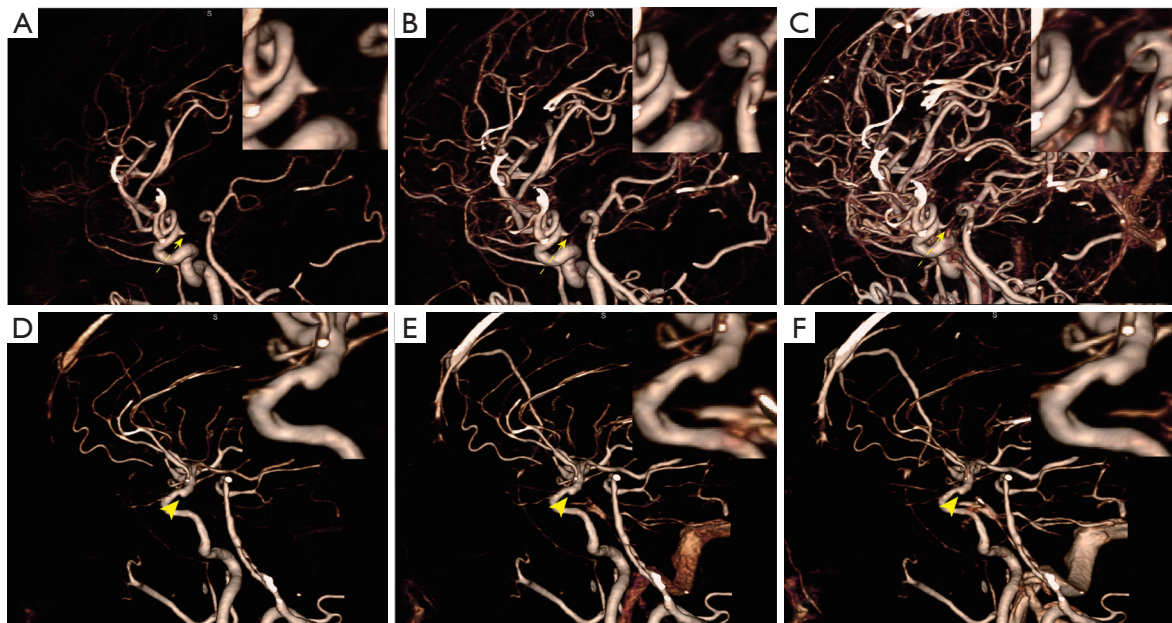


Figure 4 Comparison images of ID and IA by mCTA. (A) A pre-peak arterial image, it demonstrates a funnel-shaped symmetrical enlargement at the origin of the PcomA without the aneurysm neck. The entire PcomA is not visualized. (B,C) Display images of the peak arterial phase and late peak phase, with progressively clearer PcomA visualization (arrows). (D-F) The pre- to post-peak artery of the IA (arrows), with the arterial branch at the apex of the lesion never seen from the beginning. ID, infundibular dilation; IA, intracranial aneurysm; mCTA, multiphase computed tomography angiography; PcomA, posterior communicating artery.

posterior cerebral artery and the varying complexity of flow conditions within the PComA (7), poor heart function can also affect the filling of collaterals (27). Meanwhile, mCTA has high sensitivity and specificity in the detection of shunt lesions and can increase the display of PcomA.

Recently, mCTA has been increasingly used in clinical trials for the assessment of different neurovascular disorders as a noninvasive alternative to invasive DSA (28). It was recently studied as a time-resolved variant of CTA in which 1 arterial and 2 venous phases were obtained (28). Compared to sCTA, mCTA has a significant advantage for the evaluation of hemodynamics, especially in evaluation of the extent and dynamics of collateral flow (28). In addition, it is characterized by higher interrater reliability. In our retrospective study, mCTA dynamically displayed distal branches and had higher interrater reliability than sCTA. Contrastingly, mCTA shows dynamic information on the branching of the ID, whereas the aneurysm does not show the vessel of apex origin from the beginning (Figure 4). The display of branch arteries arising from their apex helps to distinguish ID from IA, with mCTA shown in 18 of 19 IDs in our study, the remaining case was misdiagnosed as IA because the post-processors were

not informed of the presence of the lesion and did not select the appropriate reconstruction window width and position according to the lesion. However, VR of sCTA resulted in 5 cases of misdiagnosis due to non-display of branches at the apex of the ID (Figure 5); diagnosis by source images circumvented 1 case of misdiagnosis and increased diagnostic confidence, but mCTA showed a more visual and comprehensive lesion (Figure 6), and it was relatively easy to differentiate between IA and ID ($P=0.045$). The sensitivity, specificity, PPV, NPV, and accuracy of ID identification by mCTA images were 94.7%, 87.5%, 90.0%, 93.3%, and 91.4%, respectively. It was relatively easier ($P=0.004$) and with higher confidence ($P=0.005$) for both observers to distinguish ID and IA by mCTA than by VR image of sCTA. The 5 cases misdiagnosed as IA by VR of sCTA were accurately diagnosed as ID by mCTA in 4 cases, whereas 1 of the 3 patients misdiagnosed as ID were accurately diagnosed as IA. The 4 cases misdiagnosed as IA by source images of sCTA were accurately diagnosed as ID by mCTA in 3 cases, 1 of the 3 patients misdiagnosed as ID was accurately diagnosed as IA. The NRI was 0.273 (95% CI: -0.003 to 0.566) and 0.220 (95% CI: 0.048 – 0.442), suggesting that the application of mCTA differentiated

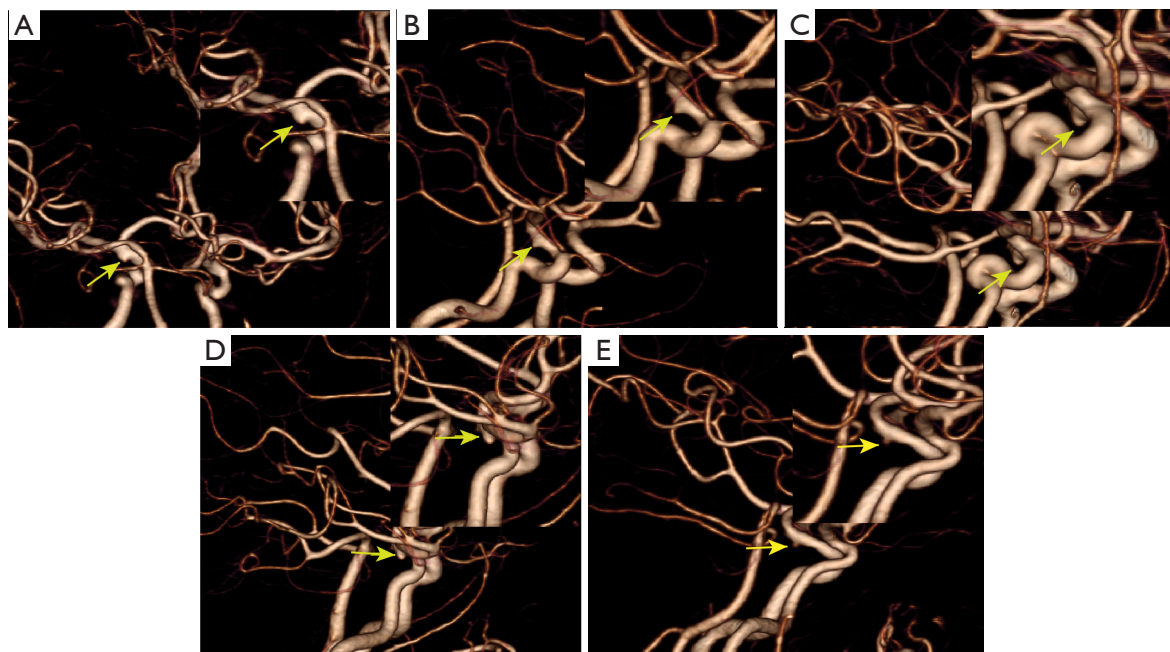


Figure 5 Images of sCTA misdiagnosis. (A-E) Demonstrate the sCTA images of 5 patients respectively, which were misdiagnosed as aneurysms because they failed to show the branches at the apex of the ID (arrows). sCTA, single-phase computed tomography angiography; ID, infundibular dilation.

between ID and IA compared to sCTA is more helpful. In addition, mCTA is non-invasive, cheaper, less time-consuming, and avoids more radiation exposure than DSA examinations. Neurological complications that may arise from DSA include reversible ischemic neurologic deficit, transient ischemia attack, and even permanent strokes (6). Compared to sCTA, mCTA with multiple acquisitions reduces the difficulty of detecting ID and distinguishing it from IA, but it should be noted that the mean estimated effective dose of mCTA is typically increased by 20% (28), even though the radiation dose for each scan is lower than that of traditional sCTA.

Screening for suspected intracranial aneurysms is often performed by MRA and routine sCTA, but MRA has a limited capability to differentiate between IA and ID at the ICA-PComA. Routine sCTA may result in misdiagnosis due to the bidirectional flow within the PComA from the distal ICA and proximal posterior cerebral artery and the varying complexity of flow conditions within the PComA (7) or poor heart function (27), causing some patients to eventually undergo DSA, which is invasive and has a high radiation dose and risk of complications such as sustained neurological dysfunction; DSA is unnecessary for ID patients. The advantages of mCTA for collateral vessels

were shown to be significant, and the use of mCTA was effective in reducing the use of DSA when it was difficult to differentiate between IA and ID by MRA or sCTA. Patients with ID need long-term follow-up, and mCTA is helpful for lesion display and changes. Our study was based on CTP examinations, which are based on multiple scans, but for follow-up patients we can scan only the peak arterial phase, peak venous phase, and late venous phase to reduce the unnecessary increase in radiation dose from multiple scans. DSA must be used with caution during follow-up. In patients with acute stroke, if a small protrusion at the ICA-PComA is detected while performing CTP, mCTA based on CTP examination can also better distinguish between IA and ID and improve the diagnostic accuracy.

There were several limitations to this study. Our study analyzed only the lesions of the ICA-PComA junction. In addition to PComA, there are many areas where it is difficult to distinguish between the actual branching vascular structure/infundibulum and the aneurysm, such as the anterior choroidal artery, anterior communicating artery, and ophthalmic artery; we will further enhance the study in the future. The retrospective design with small sample sizes, and the scanning parameters of mCTA and sCTA were not identical. Inter- or intra-observer bias may

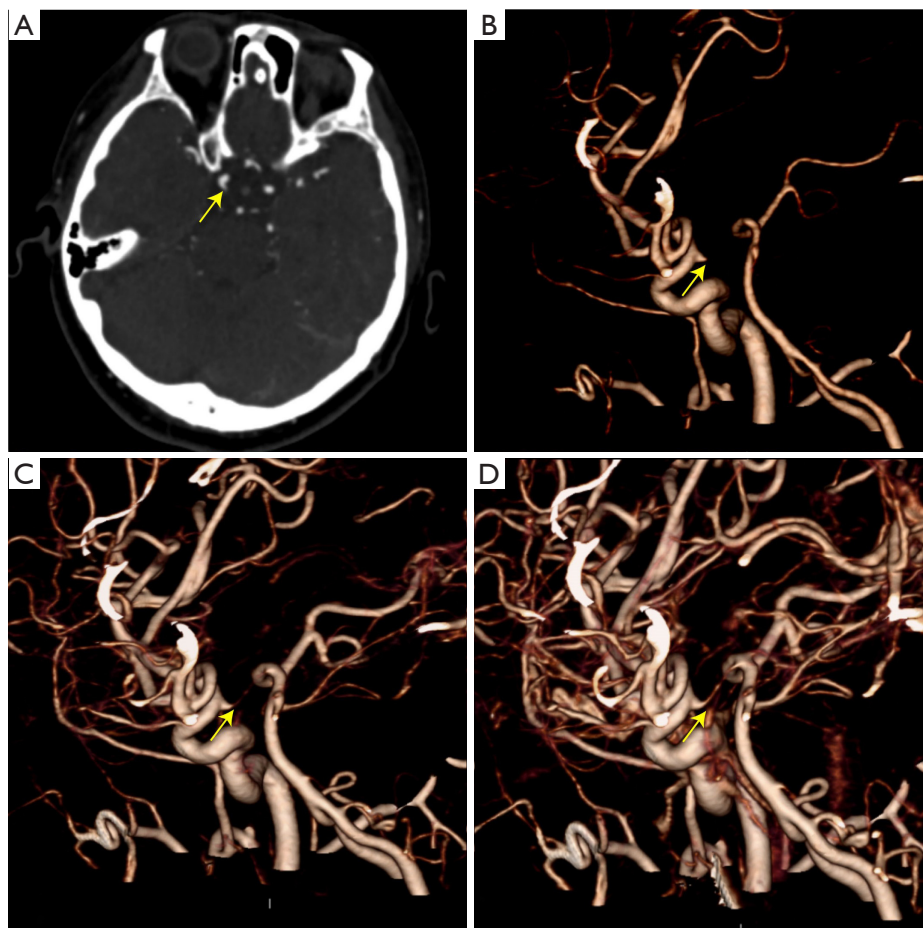


Figure 6 Comparison of source images of sCTA with VR images of mCTA. (A) The axial source image of sCTA displaying the ID (yellow arrow) at ICA–PCoM without arterial apex vessels. (B–D) VR images of mCTA, which visually and comprehensively displays the full picture of the ID (yellow arrow). sCTA, single-phase computed tomography angiography; VR, volume rendering; mCTA, multiphase computed tomography angiography; ID, infundibular dilation; ICA–PCoM, origin of the posterior communicating artery at its junction with the internal carotid artery.

have affected our results. MCTA derived from CTP data does not necessarily simulate first-line multiphase CTA (8), limiting the time of arteriographic acquisitions. Although mCTA makes it easy to display branches at the ID apex, it is difficult to avoid an increase in radiation dose as the number of acquisitions increases. Both sCTA and CTP scans in our study had a high radiation dose, which we will focus on improving in future studies. Finally, because this is a preliminary discussion, we hope that the efficacy of mCTA in identifying ID can be validated in the future through increased sample size or multi-center studies.

Conclusions

Compared to sCTA, mCTA derived from CTP data has the advantage of demonstrating the small apical branches of ID, improving diagnostic confidence and helping to differentiate between ID and IA.

Acknowledgments

Funding: This work was supported by the Clinical Study of Intracerebral Precision Transplantation of Neural Stem

Cells for Stroke (No. 2020-3-201).

Footnote

Reporting Checklist: The authors have completed the STARD reporting checklist. Available at <https://qims.amegroups.com/article/view/10.21037/qims-23-211/rc>

Conflicts of Interest: All authors have completed the ICMJE uniform disclosure form (available at <https://qims.amegroups.com/article/view/10.21037/qims-23-211/coif>). The authors have no conflicts of interest to declare.

Ethical Statement: The authors are accountable for all aspects of the work in ensuring that questions related to the accuracy or integrity of any part of the work are appropriately investigated and resolved. The study was conducted in accordance with the Declaration of Helsinki (as revised in 2013). The study was approved by the Institutional Review Board of Chinese PLA General Hospital (No. HZKY-PJ-2020-38) and the requirement for individual consent for this retrospective analysis was waived.

Open Access Statement: This is an Open Access article distributed in accordance with the Creative Commons Attribution-NonCommercial-NoDerivs 4.0 International License (CC BY-NC-ND 4.0), which permits the non-commercial replication and distribution of the article with the strict proviso that no changes or edits are made and the original work is properly cited (including links to both the formal publication through the relevant DOI and the license). See: <https://creativecommons.org/licenses/by-nc-nd/4.0/>.

References

- Huhtakangas J, Numminen J, Pekkola J, Niemelä M, Korja M. Screening of unruptured intracranial aneurysms in 50 to 60-year-old female smokers: a pilot study. *Sci Rep* 2021;11:23729.
- Rinkel GJ, Ruigrok YM. Preventive screening for intracranial aneurysms. *Int J Stroke* 2022;17:30-6.
- Bederson JB, Connolly ES Jr, Batjer HH, Dacey RG, Dion JE, Diringer MN, Duldner JE Jr, Harbaugh RE, Patel AB, Rosenwasser RH; . Guidelines for the management of aneurysmal subarachnoid hemorrhage: a statement for healthcare professionals from a special writing group of the Stroke Council, American Heart Association. *Stroke* 2009;40:994-1025.
- Griffin AS, Oppong MD, Hauck EF. Infundibular Dilations and Subarachnoid Hemorrhage: to Treat or Not to Treat? *World Neurosurg* 2019;123:188-92.
- Chen CJ, Moosa S, Ding D, Raper DM, Burke RM, Lee CC, Chivukula S, Wang TR, Starke RM, Crowley RW, Liu KC. Infundibular dilations of the posterior communicating arteries: pathogenesis, anatomical variants, aneurysm formation, and subarachnoid hemorrhage. *J Neurointerv Surg* 2016;8:791-5.
- Jang H, Jung WS, Myoung SU, Kim JJ, Jang CK, Cho KC. Source Image Based New 3D Rotational Angiography for Differential Diagnosis between the Infundibulum and an Internal Carotid Artery Aneurysm : Pilot Study. *J Korean Neurosurg Soc* 2021;64:726-31.
- Min KJ, Yoon DY, Kim HC, Lee JY, Cho BM. Infundibular dilation and aneurysm at the origin of the posterior communicating artery: differential diagnosis by CT angiography. *Neuroradiology* 2014;56:917-23.
- Wang Z, Xie J, Tang TY, Zeng CH, Zhang Y, Zhao Z, Zhao DL, Geng LY, Deng G, Zhang ZJ, Ju SH, Teng GJ. Collateral Status at Single-Phase and Multiphase CT Angiography versus CT Perfusion for Outcome Prediction in Anterior Circulation Acute Ischemic Stroke. *Radiology* 2020;296:393-400.
- Ghariq E, Mendrik AM, Willems PW, Joemai RM, Ghariq E, Vonken EJ, van Osch MJ, van Walderveen MA. Total bolus extraction method improves arterial image quality in dynamic CTAs derived from whole-brain CTP data. *Biomed Res Int* 2014;2014:603173.
- Kim EY, Shin DH, Noh Y, Goh BH, Lee YB. Comparison of Imaging Selection Criteria for Intra-Arterial Thrombectomy in Acute Ischemic Stroke with Advanced CT. *Eur Radiol* 2016;26:2974-81.
- Landis JR, Koch GG. The measurement of observer agreement for categorical data. *Biometrics* 1977;33:159-74.
- Alba AC, Agoritsas T, Walsh M, Hanna S, Iorio A, Devereaux PJ, McGinn T, Guyatt G. Discrimination and Calibration of Clinical Prediction Models: Users' Guides to the Medical Literature. *JAMA* 2017;318:1377-84.
- Lee W, Han HJ, Kim J, Choi JY, Park KY, Kim YB, Chung J. Ruptured Infundibular dilatation of the posterior communicating artery. *Acta Neurochir (Wien)* 2021;163:797-803.
- Endo S, Furuichi S, Takaba M, Hirashima Y, Nishijima M, Takaku A. Clinical study of enlarged infundibular dilation of the origin of the posterior communicating artery. *J Neurosurg* 1995;83:421-5.
- Fischer S, Hopf N, Henkes H. Evolution from an

- infundibulum of the posterior communicating artery to a saccular aneurysm. *Clin Neuroradiol* 2011;21:87-90.
16. Stuntz JT, Ojemann GA, Alvord EC Jr. Radiographic and histologic demonstration of an aneurysm developing on the infundibulum of the posterior communicating artery. Case report. *J Neurosurg* 1970;33:591-5.
 17. Pereira BJ, Holanda VM, de Holanda CV, de Oliveira JG. Intracranial aneurysm arising from infundibular dilation. *BMJ Case Rep* 2013;2013:bcr2013200115.
 18. Yu J, Wang H, Xu K, Wang B, Luo Q. Endovascular embolization of ruptured infundibular dilation of posterior communicating artery: a case report. *Case Rep Med* 2010;2010:210397.
 19. Coupe NJ, Athwal RK, Marshman LA, Brydon HL. Subarachnoid hemorrhage emanating from a ruptured infundibulum: case report and literature review. *Surg Neurol* 2007;67:204-6.
 20. Kuwahara S, Uga S, Mori K. Successful treatment of a ruptured enlarged infundibular widening of the posterior communicating artery--case report. *Neurol Med Chir (Tokyo)* 2001;41:25-8.
 21. Cloft HJ, Joseph GJ, Dion JE. Risk of cerebral angiography in patients with subarachnoid hemorrhage, cerebral aneurysm, and arteriovenous malformation: a meta-analysis. *Stroke* 1999;30:317-20.
 22. Willinsky RA, Taylor SM, TerBrugge K, Farb RI, Tomlinson G, Montanera W. Neurologic complications of cerebral angiography: prospective analysis of 2,899 procedures and review of the literature. *Radiology* 2003;227:522-8.
 23. Kaufmann TJ, Huston J 3rd, Mandrekar JN, Schleck CD, Thielen KR, Kallmes DF. Complications of diagnostic cerebral angiography: evaluation of 19,826 consecutive patients. *Radiology* 2007;243:812-9.
 24. Satoh T, Omi M, Ohsako C, Fujiwara K, Tsuno K, Sasahara W, Onoda K, Tokunaga K, Sugiu K, Date I. Differential diagnosis of the infundibular dilation and aneurysm of internal carotid artery: assessment with fusion imaging of 3D MR cisternography/angiography. *AJNR Am J Neuroradiol* 2006;27:306-12.
 25. Ebina K, Ohkuma H, Iwabuchi T. An angiographic study of incidence and morphology of infundibular dilation of the posterior communicating artery. *Neuroradiology* 1986;28:23-9.
 26. Shi WY, Li YD, Li MH, Gu BX, Wang W, Zhang BL, Li M. Infundibular dilation: an anatomical variant or a pre-aneurysm? Advantages of assessment with three-dimensional rotational angiography. *Surg Radiol Anat* 2011;33:75-80.
 27. Menon BK, d'Esterre CD, Qazi EM, Almekhlafi M, Hahn L, Demchuk AM, Goyal M. Multiphase CT Angiography: A New Tool for the Imaging Triage of Patients with Acute Ischemic Stroke. *Radiology* 2015;275:510-20.
 28. Dundamadappa S, Iyer K, Agrawal A, Choi DJ. Multiphase CT Angiography: A Useful Technique in Acute Stroke Imaging-Collaterals and Beyond. *AJNR Am J Neuroradiol* 2021;42:221-7.

Cite this article as: Zhang H, Liu W, Zhang Z, Yan Z, Tao X, Qiu F, Qiao Y, Zhang L. Multiphase computed tomography angiography derived from computed tomography perfusion data for the differential diagnosis of intracranial aneurysm and infundibular dilation. *Quant Imaging Med Surg* 2023;13(9):6105-6115. doi: 10.21037/qims-23-211